

Theoretical Study of Geometries and Electronic Transition of Color-Switching Molecules: Tetra-Aza Macrocycle and Its Zinc Complexes

Zhenxia Zhu,[1] Keiko Takano,*[1] Ayako Furuhama,[1] Shojiro Ogawa,[1] and Shinji Tsuchiya[2]

[1]Graduate School of Humanities and Sciences, Ochanomizu University, 2-1-1 Otsuka, Bunkyo-ku, Tokyo 112-8610

[2]Institute of Industrial Science, The University of Tokyo, 7-22-1 Roppongi, Minato-ku, Tokyo 106-0032

Received August 9, 2006; E-mail: takano.keiko@ocha.ac.jp

Tetra-aza macrocycles containing 2,2′-bipyridine moieties fascinatingly undergo color-switching. Here, a tetra-aza macrocycle was analyzed as well as its zinc complexes from the viewpoint of ab initio molecular orbital (MO) and density functional theory (DFT) calculations. As a result of systematic geometry searches, obtained geometries of stable conformers were consistent with the structural formula developed from the experimental results. Transition energies and oscillator strengths of the stable conformers were calculated based on time-dependent DFT (TDDFT) and compared with the experimental data. The effect of the solvent was considered by using a polarization continuum model (PCM). The calculated transition energies qualitatively agreed with the experimental UV spectra. Structural changes upon complexation and the features of the molecular orbitals related to the transition from the ground state to the excited states are discussed.

Macrocycles with a stable and selective ionophore for metal cations are rather important for practical applications, such as serving as chemical sensors.[1] We have been investigating such tetra-aza macrocycles with pyridyl-based ligands from both the experimental[2–5] and theoretical[6–8] points of view. We have reported the fascinating property of color-switching involving tetra-aza macrocycles containing 2,2′-bipyridine.[5] The color of the solution containing the free macrocycle is orange in dichloromethane (CH_2Cl_2), acetonitrile (CH_3CN), or methanol (CH_3OH), which corresponds to similar absorption peaks of experimental spectra. Thus, it is speculated that they have similar geometries. In contrast, its zinc complexes have different colors depending on the solvent, which means they might have different geometries in each solution. In other words, when macrocycle **1** reacts with $ZnCl_2$ in CH_2Cl_2, in CH_3CN, or in CH_3OH, the products or geometries might be different from each other. Structural formulae developed from our previous experiments are shown in Chart 1. Experimental investigation has shown that the color of the solution and the UV–visible spectrum of the zinc complexes are altered by the addition of acids or bases and that such transformations are reversible.

Geometries of such fascinating macrocyclic species, to the best of our knowledge, have not yet been reported. Thus, it is important to conduct analyses of the geometries of these species; in particular, it is of interest to investigate the spectroscopically observed features associated with the conformational changes of macrocycle **1** and its zinc complexes (Chart 1) from a theoretical point of view. In the present study, the geometric features of the macrocycle and the corresponding metal complexes, the energy profiles of the UV–visible spectra, and the relationship between the geometric and spectroscopic features were investigated by ab initio molecular orbital (MO) and density functional theory (DFT) calculations. In addition, solvent effects were investigated using a polarizable continuum model (PCM) combined with time-dependent DFT calculations (TDDFT-PCM).

Geometrical Features of the Studied Molecules

Macrocyclic species studied in this paper have several possible conformations as expected by the structural formulae shown in Chart 1. For macrocycle **1**, there are two possibilities for mutual orientation of the functional groups, i.e., a CN

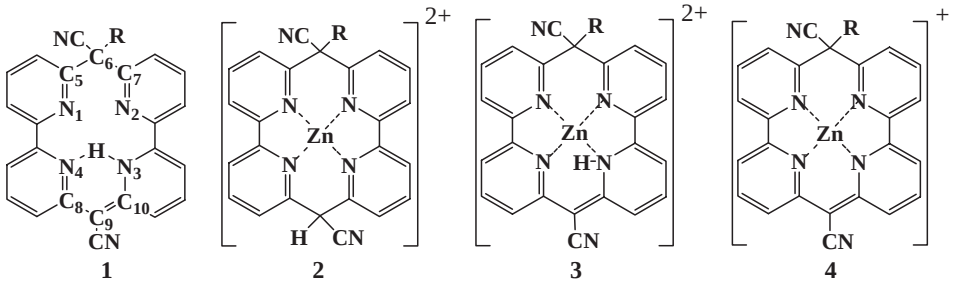

Chart 1. Structural formulae of macrocycle **1** and zinc complexes **2**–**4**.

Published on the web April 13, 2007; doi:10.1246/bcsj.80.686

group can exist outside or inside the macrocyclic moiety on the bridging sp^3 carbon atom. Furthermore, in each case, the alkyl group can rotate around the C_6–C_α bond connecting the bridging carbon atom, C_6, and the C_α atom of the alkyl group. Complexes **3** and **4** are similar to macrocycle **1** in both of the two bridging carbon atoms, i.e., sp^2 and sp^3 carbons. In contrast, complex **2** has another sp^3 carbon atom on the opposite side of the alkyl group. Therefore, the orientations of the CN groups on the both sides have to be considered in this case.

Computational Details

Geometry searches were carried out for metal-free tetra-aza macrocycle **1** containing 2,2′-bipyridine and having a hydrogen atom inside the macrocyclic moiety (see Chart 1). Due to the calculation cost, molecules containing a butyl group instead of a dodecyl group, which has been previously experimentally investigated,[5] were selected for all calculations. Preliminary semi-empirical molecular orbital, PM3, calculations[9] were carried out for the two cases with a CN group outside and inside after minimum energy path calculations for the C_6–C_α bond rotation connecting the bridging carbon atom, C_6, and the C_α atom of the alkyl group in macrocycle **1**. For several local minimum structures of macrocycle **1** on the minimum energy paths from the PM3 calculations, geometry optimizations were performed at the restricted Hartree–Fock (RHF) level of theory with the 3-21G[10] and 6-31G*[11] basis sets.

Geometry searches of stable conformers of the metal complexes **3** and **4** were also carried out in relation to the results for the free macrocycle **1** due to the similarity among **1**, **3**, and **4** in the hybridization-types of the bridging carbon atoms. For complex **2**, the orientation of the CN group on the bridging sp^3 carbon atom on the opposite side of the alkyl group was also considered. Geometries of macrocycle **1** and zinc complexes **2**–**4** were also optimized based on DFT, B3LYP/6-31G*. The B3LYP functional[12a] uses a three-parameter exchange functional from Becke (B3)[12b] and the Lee, Yang, and Parr (LYP) correlation gradient-corrected functional.[12c] Force constant matrices (Hessians) were further calculated for all the RHF stationary points in order to identify them as minima (all positive constants), transition states (one negative force constant), or higher-order saddle points.

In order to consider solvent effect on relative energies of the stable conformers, single-point energy B3LYP/6-31G* calculations with PCM (SP-PCM), were also carried out using the B3LYP/6-31G* optimized geometries of the zinc complexes.

To study the color variation, transition energies, and oscillator strengths were calculated by TDDFT[13,14] combined with the PCM to consider solvent effect at the B3LYP/6-31G* optimized geometries.

PM3 calculations involving the minimum energy paths for the C_6–C_α bond rotation in macrocycle **1** were carried out using the BioMedCAChe program.[15] The Gaussian03 program[16] was used for geometry optimizations and Hessian calculations by ab initio RHF and DFT methods and transition energy calculations by TDDFT using the PCM. The MolStudio program[17] was used for visualizing the structures and vibrational modes. The Gnuplot program was used to draw the graphs in Fig. 3.

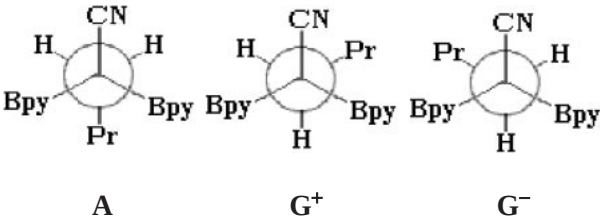

Fig. 1. Newman projections of the conformers of macrocycle **1** around the C_6 (see Chart 1) and C_α next to C_6 in the butyl group. Bpy denotes bipyridine moiety connected to the C_6 atom. Pr denotes propyl group bonded to C_α atom.

Table 1. Energies (ΔE in kcal mol^{-1}) of Conformers of Metal-Free Macrocycle **1** to the $\mathbf{CN_{out}}$-$\mathbf{G^+}$ Conformer

Conformer	ΔE (RHF/3-21G)	ΔE (RHF/6-31G*)	ΔE (B3LYP/6-31G*)
1(CN_{out}-G^+)	0	0	0
1(CN_{out}-G^-)	0.1	0.0	0.1
1(CN_{out}-A)	5.3	5.5	4.4
1(CN_{in}-G^-)	8.2	7.4	6.8
1(CN_{in}-G^+)	7.9	7.2	6.9

Results and Discussion

Optimized Geometries of the Metal-Free Macrocycle. As a preliminary result of PM3 calculations for minimum energy paths, six local minima of macrocycle **1** were found. They were denoted as **1(CN_{out}-A)**, **1(CN_{out}-G^+)**, **1(CN_{out}-G^-)**, **1(CN_{in}-A)**, **1(CN_{in}-G^+)**, and **1(CN_{in}-G^-)** according to two kinds of categories. One was based on the orientation of the CN group, i.e., outward and inward, respectively, denoted as CN_{out} and CN_{in}. The other was based on the conformation around the C_6–C_α single bond between the bridging C atom, C_6, and the C_α next to C_6 in the butyl group. Figure 1 shows Newman projections for the anti (A) and gauche (G^+ and G^-) conformers of macrocycle **1**. For example, **1(CN_{out}-A)** has a propyl group at the anti-position (A) against the outside CN group. Among the six local minima of macrocycle **1** from the PM3 calculations, the geometry of **1(CN_{in}-A)** led to the same optimized geometry as **1(CN_{out}-A)** at the RHF level of theory with the 3-21G and 6-31G* basis sets. Relative energies of the five conformers are listed in Table 1. The CN_{out} conformers were more stable than the CN_{in} ones. This is attributed to the repulsive interaction between the CN group and the N atoms in the bipyridine moieties for the former conformers. The gauche conformers G^+ and G^- were similar in energy among the conformers with a CN group pointing in the same direction. Namely, **1(CN_{out}-G^+)** and **1(CN_{out}-G^-)** as well as **1(CN_{in}-G^+)** and **1(CN_{in}-G^-)** were quite similar in energy. Gauche conformers **1(CN_{out}-G^+)** and **1(CN_{out}-G^-)** were more stable than **1(CN_{out}-A)** and the most stable among the metal-free conformers. The reason for the stability of G^+ and G^- can be explained by steric factors. As shown in Fig. 1, the bulky propyl group (**Pr**) in **A** is gauche to the two another bulky bipyridine moieties (**Bpy**), while the propyl group in $\mathbf{G^+}$ and $\mathbf{G^-}$ is anti and gauche to each bipyridine moiety. Thus, **A** seems to be less stable because of steric effect. Relative energies of the DFT optimized geometries were similar to those from the

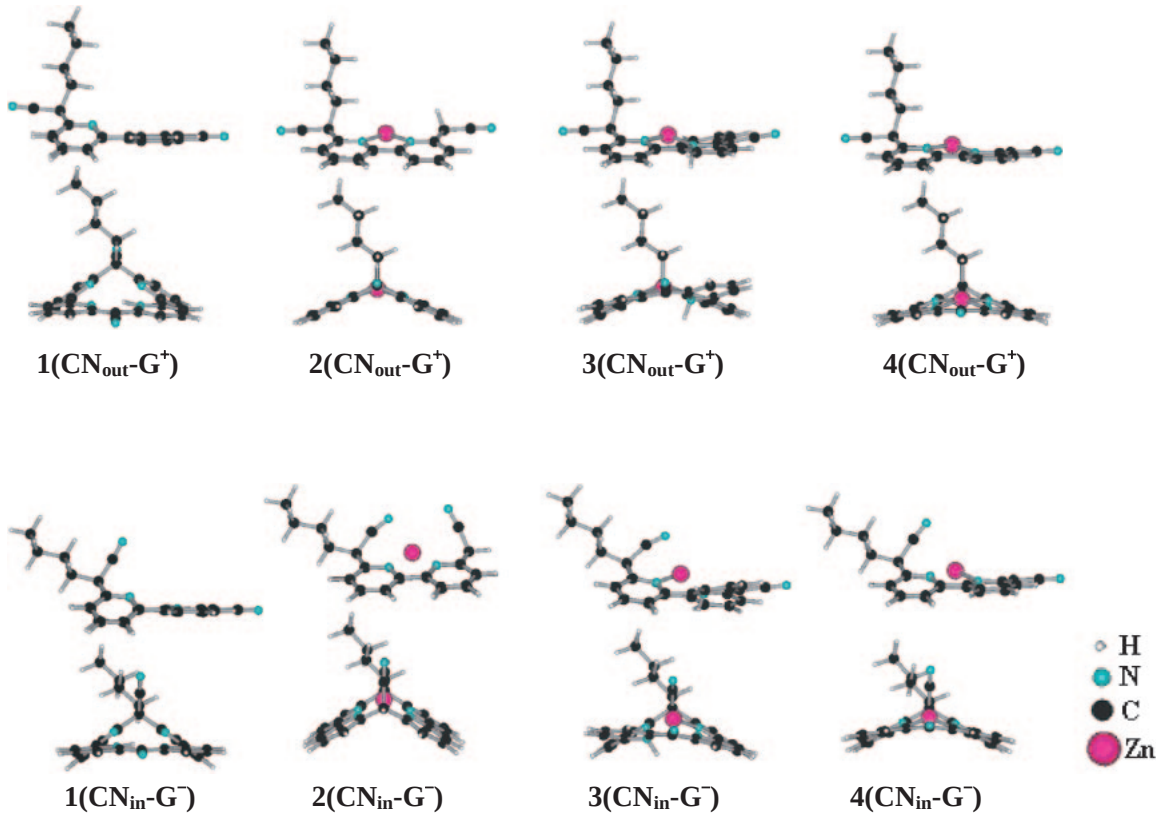

Fig. 2. Side views from the two directions of $\mathbf{CN_{out}\text{-}G^+}$ and $\mathbf{CN_{in}\text{-}G^-}$ of macrocycle **1** and zinc complexes **2**–**4** as isolated molecules on the B3LYP/6-31G* potential energy surfaces.

RHF calculations, though the values were slightly smaller (see Table 1). The DFT-optimized structure of the most stable conformer $\mathbf{1(CN_{out}\text{-}G^+)}$ is shown from the two viewpoints in Fig. 2. That of $\mathbf{1(CN_{in}\text{-}G^-)}$ is also depicted for reference.

To confirm the stability of macrocycle **1** having an inside hydrogen atom attached to the nitrogen atom in bipyridines and having a planar-conjugated part (see Chart 1 and Fig. 2), additional geometry optimizations were carried out for an isomer possessing a hydrogen atom connected to the bridging carbon atom C_9 (see the structural formula of **1** in Chart 1). The resultant isomer had two sp^3 bridging carbon atoms. As a result, the obtained isomer seemed to be less stable because of a lack of conjugation with non-planar geometries. Geometry searches of the isomer having an outside-hydrogen were successful at the RHF level of theory with the 3-21G basis set. It was found to be a local minimum based on the vibrational analysis and to be less stable in energy by ca. 20 kcal mol^{-1} than the most stable isomer having a hydrogen atom inside, $\mathbf{1(CN_{out}\text{-}G^+)}$. This energy difference is consistent with the fact that the isomer having an outside-hydrogen connected to C_9 has not been found, but only one of the isomers having an inside-hydrogen, which is shown as macrocycle **1** in Chart 1, has been observed to date.

Geometries of Zinc Complexes. Geometry searches of local minimum structures were carried out for the conformers of complex **3** by adding a Zn cation (Zn^{2+}) to macrocycle **1** at the RHF level of theory with the 3-21G basis set. Since conformers $\mathbf{1(CN_{out}\text{-}G^+)}$ and $\mathbf{1(CN_{out}\text{-}G^-)}$ as well as $\mathbf{1(CN_{in}\text{-}G^+)}$ and $\mathbf{1(CN_{in}\text{-}G^-)}$ were similar in energy, only the three local minima of macrocycle $\mathbf{1(CN_{out}\text{-}G^+)}$, $\mathbf{1(CN_{out}\text{-}A)}$, and $\mathbf{1(CN_{in}\text{-}G^-)}$ were used as starting conformations for the zinc complexes. Geometry searches of the Zn complexes of the three conformers $\mathbf{3(CN_{out}\text{-}G^+)}$, $\mathbf{3(CN_{out}\text{-}A)}$, and $\mathbf{3(CN_{in}\text{-}G^-)}$ were successful. The optimized geometries of the three conformers were found to be local minima based on Hessian calculations. Conformers $\mathbf{3(CN_{out}\text{-}G^+)}$ and $\mathbf{3(CN_{out}\text{-}A)}$ were similar in energy to each other at the RHF/3-21G level of theory (see Table 2). Conformer $\mathbf{3(CN_{out}\text{-}A)}$ converged on $\mathbf{3(CN_{out}\text{-}G^+)}$ during the more reliable B3LYP/6-31G* geometry optimization. The same change in the conformers from $\mathbf{CN_{out}\text{-}A}$ to another gauche conformer by B3LYP/6-31G* calculations was also seen for complexes **2** and **4**. Therefore, only $\mathbf{CN_{out}\text{-}G^+}$ and $\mathbf{CN_{in}\text{-}G^-}$ were considered for single-point energy calculations involving zinc complexes **2**–**4**, using SP-PCM.

Relative energies among the conformers calculated at the RHF/3-21G and B3LYP/6-31G* levels in the gas phase without solvent and at the B3LYP/6-31G* level using SP-PCM are listed in Table 2. The B3LYP/6-31G* local minimum structures, i.e., $\mathbf{CN_{out}\text{-}G^+}$ and $\mathbf{CN_{in}\text{-}G^-}$, of macrocycle **1** and zinc complexes **2**–**4** as isolated molecules in gas phase are depicted from the two viewpoints in Fig. 2. Lone pairs of the four pyridine nitrogens coordinate to the central zinc cation. In gas phase, conformer $\mathbf{2(CN_{in}\text{-}G^-)}$ was more stable than conformer $\mathbf{2(CN_{out}\text{-}G^+)}$ by 9.2 (13.1) kcal mol^{-1} according to the B3LYP/6-31G* (RHF/3-21G) calculations. Coulomb interaction between the cationic zinc and the electronegative cyano group could be favorable in this complex as an isolated molecule. Using SP-PCM reduced the energy difference between

them from 9.1 kcal mol^{-1} in gas phase to 0.1 kcal mol^{-1} in CH_2Cl_2. In other words, conformer **2(CN$_{out}$-G$^+$)** had relatively more stabilized than **2(CN$_{in}$-G$^-$)** by solvation. As a result, the stability of **2(CN$_{out}$-G$^+$)** and **2(CN$_{in}$-G$^-$)** appeared to be almost the same in CH_2Cl_2. A similar result was obtained for zinc complex **3**. Conformer **3(CN$_{out}$-G$^+$)** was more relatively stabilized than **3(CN$_{in}$-G$^-$)** by solvent effect in CH_3CN. Thus, **3(CN$_{out}$-G$^+$)** was likely to be more stable than **3(CN$_{in}$-G$^-$)**. As for zinc complex **4**, the most stable conformer **4(CN$_{out}$-G$^+$)** in gas phase at the B3LYP/6-31G* level was relatively more stabilized than the other conformers and it was the most stable in CH_3OH. The reason for the instability of **4(CN$_{in}$-G$^-$)** could be partly due to having the longer distance between the CN group and the zinc atom than that in **2(CN$_{in}$-G$^-$)** and **3(CN$_{in}$-G$^-$)**.

Table 2. Energies (ΔE in kcal mol^{-1}) of Conformers of Zinc Complexes Based on the RHF/3-21G, B3LYP/6-31G* Geometry Optimization and Single-Point Energy B3LYP/6-31G* Calculations at the B3LYP/6-31G* Geometry Using the PCM, i.e., SP-PCM Calculations

Conformer	ΔE[a)] (RHF/3-21G)	ΔE[a)] (B3LYP/6-31G*)	ΔE (SP-PCM)
2(CN$_{out}$-G$^+$)	0	0	0[b)]
2(CN$_{out}$-A)	—[e)]	—[e)]	
2(CN$_{in}$-G$^-$)	−13.1	−9.2	−0.1[b)]
3(CN$_{out}$-G$^+$)	0	0	0[c)]
3(CN$_{out}$-A)	−0.1	—[e)]	
3(CN$_{in}$-G$^-$)	−6.1	−5.3	5.7[c)]
4(CN$_{out}$-G$^+$)	0	0	0[d)]
4(CN$_{out}$-A)	2.1	—[e)]	
4(CN$_{in}$-G$^-$)	−0.5	1.8	6.1[d)]

a) In gas phase. b) In CH_2Cl_2, $\varepsilon = 8.93$. c) In CH_3CN, $\varepsilon = 36.64$. d) In CH_3OH, $\varepsilon = 32.63$. e) Conformer **CN$_{out}$-A** reached the other conformer **CN$_{out}$-G$^+$** during the geometry search.

Selected geometric parameters at the B3LYP/6-31G* level are listed in Table 3 for the **CN$_{out}$-G$^+$** conformers of macrocycle **1** and zinc complexes **2**–**4** in the gas phase. It is noteworthy that **2(CN$_{out}$-G$^+$)** has a specific feature in the macrocyclic moiety: (1) two sp^3 bridging carbon atoms, which corresponds to θ values of 113.6 and 114.9°, which is close to the ideal tetrahedral angle 109.5° and (2) coplanarity between the two bipyridine moieties, which corresponds to very small ϕ values (0.3 and −2.1 in Table 3) (see Fig. 2 also). The macrocyclic moiety of **4** had higher planarity than that of **3**. A zinc atom was buried in the macrocyclic moiety in the case of **4**. Therefore, there may be less interaction with the cyano group in compex **4** than in complex **3**. The orientation of the functional groups, i.e., cyano and butyl groups, exerts little influence on the stability of the complexes, which may account for the small difference in energy among the conformers of **4** in the gas phase (see Table 2).

Transition Energies and Oscillator Strengths of Macrocycle 1 and Its Zinc Complexes as Determined by TDDFT Calculations. **CN$_{out}$-G$^+$** conformers were found to be the most stable except for zinc complex **2**, of which isomer **CN$_{in}$-G$^-$** was also stable. Therefore, the optimized structures of the **CN$_{out}$-G$^+$** conformers were used for transition-energy calculations of all of the species studied. Using the B3LYP/6-31G* geometries of macrocycle **1(CN$_{out}$-G$^+$)** and complexes **2(CN$_{out}$-G$^+$)**, **3(CN$_{out}$-G$^+$)**, and **4(CN$_{out}$-G$^+$)**, transition energies and oscillator strengths were evaluated by using TDDFT (B3LYP/6-31G*) calculations. Table 4 lists some of the calculated transition energies λ of macrocycle **1** and zinc complexes **2**–**4** as determined by TDDFT (B3LYP/6-31G*) calculations in the gas phase and with solvent effects in comparison with the experimental data,[5] though the experimental geometries of the studied species are not known. Calculated oscillator strengths are related to experimental absorption coefficients according to the following equation:

Table 3. Selected Geometric Parameters of the **CN$_{out}$-G$^+$** Conformers of Macrocycle **1** and Zinc Complexes **2**–**4** at the B3LYP/6-31G* Level in the Gas Phase

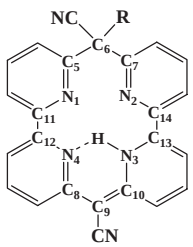

	1(CN$_{out}$-G$^+$)	**2(CN$_{out}$-G$^+$)**	**3(CN$_{out}$-G$^+$)**	**4(CN$_{out}$-G$^+$)**
r(N$_1$–Zn)/Å	—	2.020	1.989	2.041
r(N$_2$–Zn)/Å	—	2.019	2.008	1.964
r(N$_3$–Zn)/Å	—	2.033	2.173	1.965
r(N$_4$–Zn)/Å	—	2.032	1.995	2.039
r(N$_1$–N$_3$)/Å	3.921	3.954	4.027	3.954
r(N$_2$–N$_4$)/Å	3.891	3.948	3.897	3.952
θ(C$_5$–C$_6$–C$_7$)/°	108.7	113.6	114.3	114.8
θ(C$_8$–C$_9$–C$_{10}$)/°	126.0	114.9	128.6	128.7
ϕ(N$_1$–C$_{11}$–C$_{12}$–N$_4$)/°	−33.0	0.3	−14.5	−13.9
ϕ(N$_3$–C$_{13}$–C$_{14}$–N$_2$)/°	26.0	−2.1	28.8	12.8

Table 4. Calculated Transition Energies λ of Macrocycle **1** and Zinc Complexes **2–4** as Determined by TDDFT (B3LYP/6-31G*) Calculations in the Gas Phase and with Solvent Effects in Comparison with the Experimental Data[5]

	(Solvent)	λ in nm with [f] or ($\varepsilon \times 10^{-4}\,M^{-1}\,cm^{-1}$)			
1(CN_{out}-G^+)	Calc.(gas phase)[a]	259 [0.16]	349 [0.33]	415 [0.02]	517 [0.06]
	Calc.(CH_2Cl_2)[b]	262 [0.20]	344 [0.43]	393 [0.04]	471 [0.10]
	Exp.(CH_2Cl_2)[b]	281 (1.49)	359 (1.42)	378 (1.07)	464 (0.85)
	Calc.(CH_3CN)[c]	261 [0.20]	341 [0.40]	390 [0.04]	463 [0.10]
	Exp.(CH_3CN)[c]	283 (1.42)	355 (1.39)	378 (1.07)	458 (0.53)
	Calc.(CH_3OH)[d]	261 [0.21]	341 [0.40]	391 0.03]	463 [0.10]
	Exp.(CH_3OH)[d]	282 (1.34)	351 (1.41)	378 (0.97)	452 (0.50)
2(CN_{out}-G^+)	Calc.(gas phase)[a]	292 [0.19]			
	Calc.(CH_2Cl_2)[b]	294 [0.27]			
	Exp.(CH_2Cl_2)[b]	303 (2.75)			
3(CN_{out}-G^+)	Calc.(gas phase)[a]	309 [0.11]	367 [0.05]	491 [0.15]	
	Calc.(CH_3CN)[c]	296 [0.25]	356 [0.08]	477 [0.23]	
	Exp.(CH_3CN)[c]	298 (2.25)	357 (1.81)	440 (1.05)	
4(CN_{out}-G^+)	Calc.(gas phase)[a]	283 [0.40]	369 [0.21]	617 [0.11]	
	Calc.(CH_3OH)[d]	278 [0.62]	353 [0.23]	532 [0.14]	
	Exp.(CH_3OH)[d]	287 (2.50)	381 (2.63)	468 (1.05)	

The experimental spectra[5] and results of TDDFT calculations with PCM were determined in the gas phase and in the different solvents: a) in the gas phase, b) in CH_2Cl_2, c) in CH_3CN, d) in CH_3OH, respectively. Calculated oscillator strengths and experimental absorption coefficients were listed in square brackets and in parentheses, respectively.

$$f \cong 4.32 \cdot 10^{-9} \varepsilon_{max} \Delta\omega_{1/2}, \quad (1)$$

where ε_{max} is the experimental absorption coefficient with the unit of $M^{-1}\,cm^{-1}$ and $\Delta\omega_{1/2}$ corresponds to the halfwidth of the absorption band with the unit of cm^{-1}.[18] Thus, oscillator strengths are approximately proportional to absorption coefficients.

Calculated transition energies for isolated species, which corresponds to the transition energies of the molecules in the gas phase, differed greatly from the experimental values in solution. Difference in transition energies between the calculated values in the gas phase and the experimental values in solution was from ±4 to ±22 nm except for the longest wavelengths of **4**(CN_{out}-G^+) (+149 nm) and **3**(CN_{out}-G^+) (+51 nm). TDDFT-PCM calculations, which include solvent effects, improved the evaluation of the transition energies (wavelengths λ in nm), and much better agreement between the calculated transition energies and the corresponding experimental values was reached. In the worst case, the transition energy for the longest wavelength of **4**(CN_{out}-G^+) was greatly improved from 617 nm estimated in the gas phase to 532 nm in CH_3OH by 85 nm using TDDFT-PCM, though it was still different from the experimental value (468 nm). The longest-wavelength peak of **3**(CN_{out}-G^+) also changed drastically. From TDDFT-PCM, a better value of 477 nm was obtained, which is closer to the experimental value 440 nm in CH_3CN compared to the calculated value in the gas phase (491 nm). Namely, the estimated transition energy improved by 14 nm using a solvation model. For macrocycle **1**, the change in the transition energies and oscillator strengths by different solvents was small, which agreed with the experimental data.

Calculated transition energies of macrocycle **1** and zinc complexes **2–4** obtained by the TDDFT (B3LYP/6-31G*-PCM) calculations in the same solvent as the experimental absorption spectra are shown in Fig. 3. The calculated values have a general resemblance to the experimental spectra. Especially, there is a good correspondence between them for macrocycle **1** and zinc complex **2** in CH_2Cl_2 (see Figs. 3a and 3b). For zinc complex **2**, the main peak at 303 nm had shoulders, which appeared to correspond to the calculated peaks at 320 and 275 nm. The contrast between macrocycle **1** and zinc complex **2**, in other words, before and after the complexation, is described as follows: (1) the absorption peaks in the longer-wavelength region disappeared, and a peak at 294 nm appeared, and (2) the absorption bands were dense in the region from 250 to 320 nm in the zinc complex. The longest-wavelength peak of the zinc complex was outside of the visible region. These results were in agreement with the experimental results showing a change in color of the solution from orange to colorless. In regards to this experimental spectral change, Ogawa has reported that a broad band between 430 and 590 nm almost disappears, and a new peak appears at 303 nm upon formation of zinc complex **2** from free macrocycle **1**. Upon complexation in another solvent CH_3CN, formation of zinc complex **3** and the color change of the solution from orange to yellow have been reported, and the broad band in the visible region has been reported to be blue-shifted from 458 to 440 nm (see experimental data in Table 4). Two peaks of the calculated results, 436 and 477 nm corresponded to the peak of 440 nm (see Fig. 3c). Upon formation of zinc complex **4** from macrocycle **1** in CH_3OH, the experimental data showed that the broad band in the visible region red-shifted from 452 to 468 nm, as listed in Table 4, and the color of solution turned from orange to red. The longest-wavelength peak calculated by TDDFT-

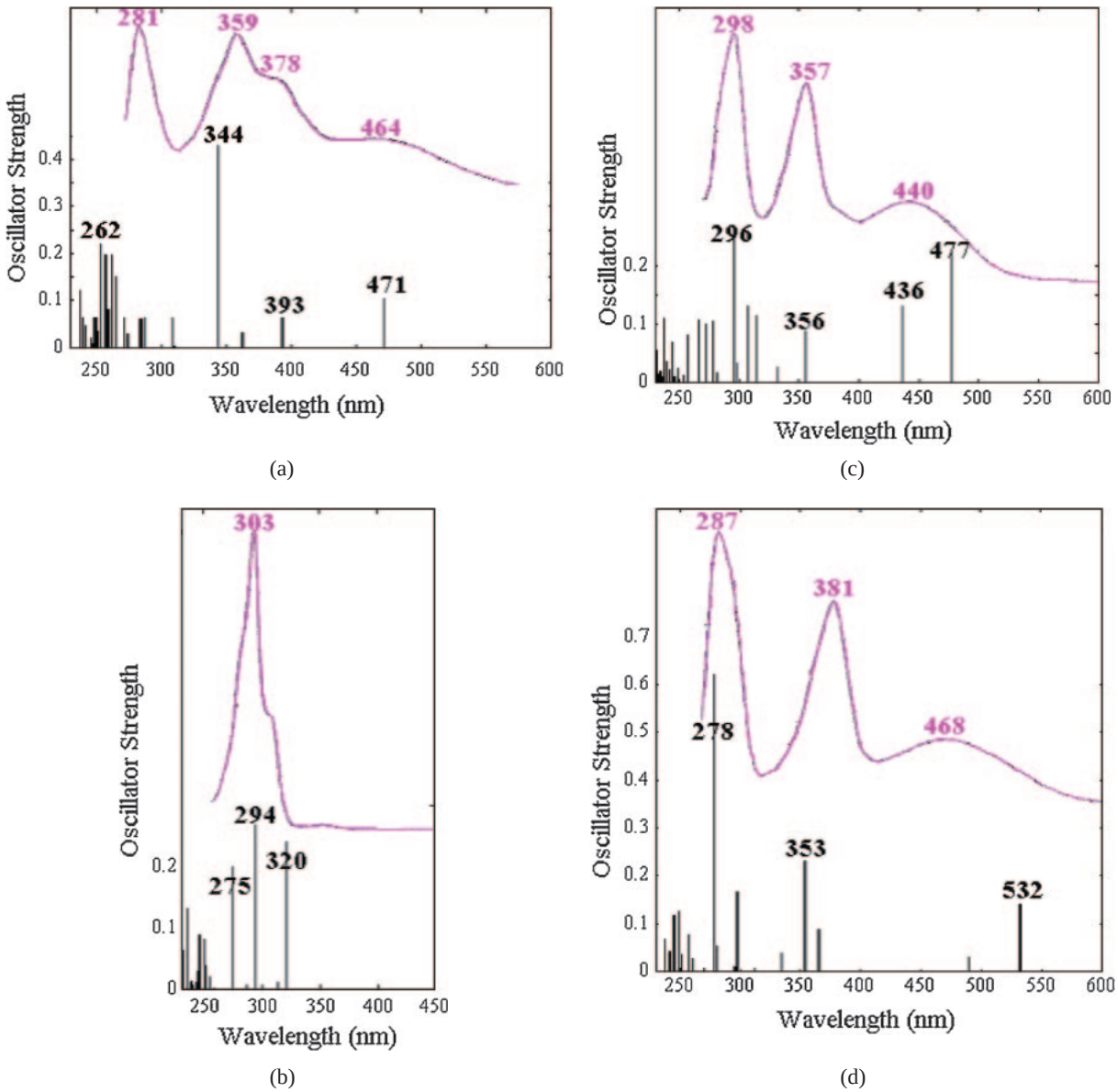

Fig. 3. Transition energies as absorption wavelengths in nm and oscillator strengths of macrocycle **1** and zinc complexes **2**–**4** as determined by B3LYP/6-31G* calculations for the structure denoted as $\mathbf{CN_{out}\text{-}G^{+}}$ shown in Fig. 2 with the experimental absorption sperctra depicted at the upper part for comparison; (a) macrocycle **1** in CH_2Cl_2 (b) zinc complex **2** in CH_2Cl_2; (c) zinc complex **3** in CH_3CN; (d) zinc complex **4** in CH_3OH.

Table 5. Main Components of the Electronic Excitation and their CI Coefficients for the Longest Wavelength as Determined by TDDFT (B3LYP/6-31G*) in the Gas Phase as an Isolated Molecule and in Solvent Based on the PCM Calculations

	Components of the first excited state	CI coefficients			
		In gas phase	In CH_2Cl_2	In CH_3CN	In CH_3OH
1($\mathbf{CN_{out}\text{-}G^{+}}$)	HOMO → LUMO	0.671	0.674	0.673	0.673
2($\mathbf{CN_{out}\text{-}G^{+}}$)	HOMO → LUMO	0.656	0.657		
	HOMO−4 → LUMO	0.157			
	HOMO−2 → LUMO		0.199		
3($\mathbf{CN_{out}\text{-}G^{+}}$)	HOMO → LUMO	0.597		0.634	
	HOMO → LUMO+1	0.226		−0.118	
4($\mathbf{CN_{out}\text{-}G^{+}}$)	HOMO → LUMO	0.659			0.674

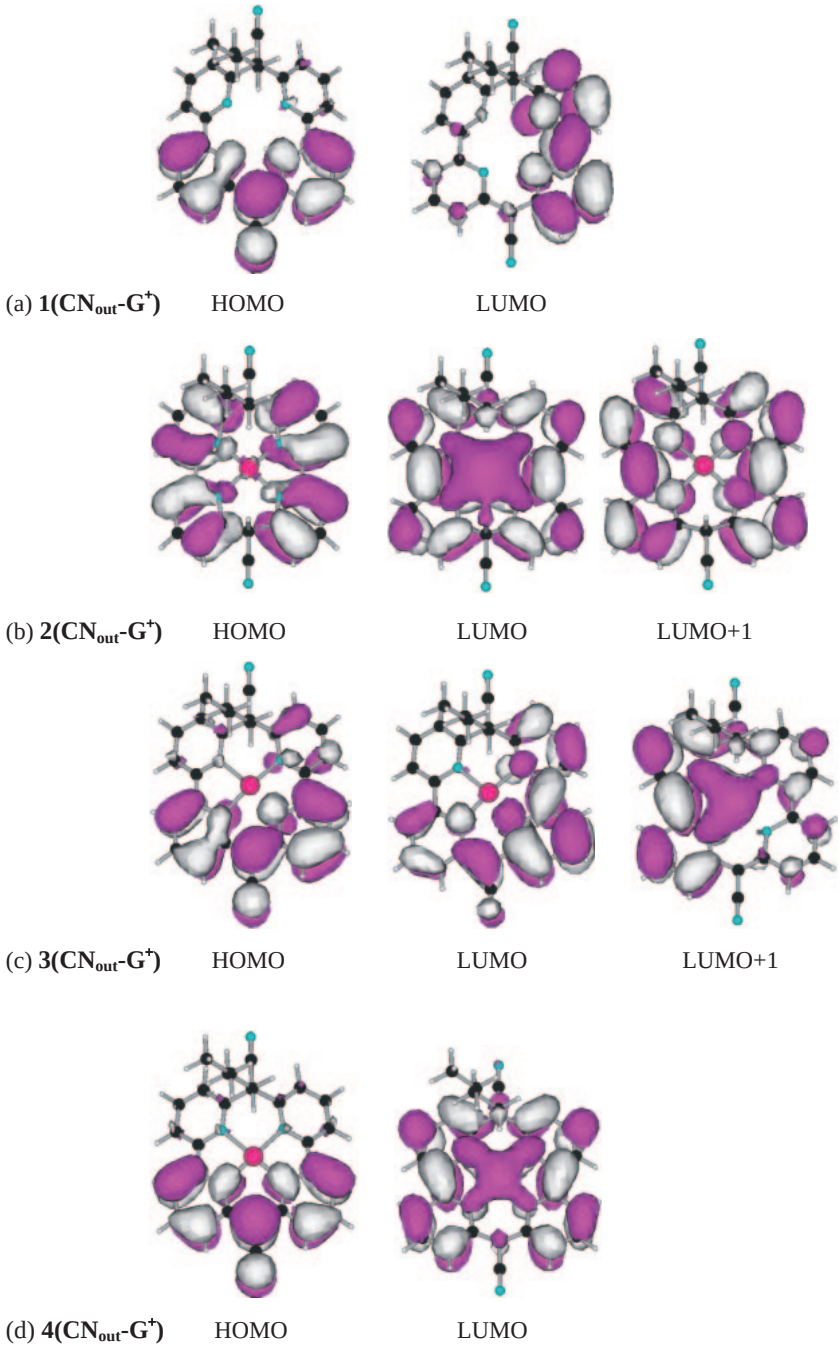

Fig. 4. Frontier orbitals of macrocycle **1** and its zinc complexes based on TDDFT-PCM calculations including the solvent effects: (a) **1(CN$_{out}$-G$^+$)** in CH_2Cl_2, (b) **2(CN$_{out}$-G$^+$)** in CH_2Cl_2, (c) **3(CN$_{out}$-G$^+$)** in CH_3CN, (d) **4(CN$_{out}$-G$^+$)** in CH_3OH.

PCM in CH_3CN was shifted from 463 nm for **1** to 532 nm for **4**. Though TDDFT-PCM overestimated the peak wavelength for **4** ($\lambda_{exp} = 468$ nm), the other two peaks in Fig. 3d were estimated well. The computational results exhibited the same trends as the experimental data, as mentioned above. Thus, the profiles of the calculated spectra obtained by the TDDFT calculations agreed semi-quantitatively with the experimental profiles.

Complex **2** showed no absorption bands in the region longer than 330 nm (Fig. 3b), in contrast to the other complexes (Figs. 3a, 3c, and 3d). Table 5 lists the main CI components of the electronic excitation to the first excited states of **1**–**4**, with their CI coefficients. The main CI components were the HOMO–LUMO excitations for **1**–**4**. The HOMOs and LUMOs of each species were compared with one another. Frontier orbitals depicted in Fig. 4 and the HOMO–LUMO gaps shown in Fig. 5 were found to be similar among **1**, **3**, and **4**. The HOMOs of **1**, **3**, and **4** were π-orbitals located in one-half of the planar region in the macrocyclic skeleton, i.e., in the two bipyridines. Furthermore, these HOMOs were similar to one another (see Fig. 4). In contrast, the MO shape of zinc complex **2** shown in Fig. 4b was different from that of **3** shown in Fig. 4c, namely, it was spread across the entire macrocyclic moiety and had an almost equivalent distribution for each pyridine ring. This feature is due to the electronic structure char-

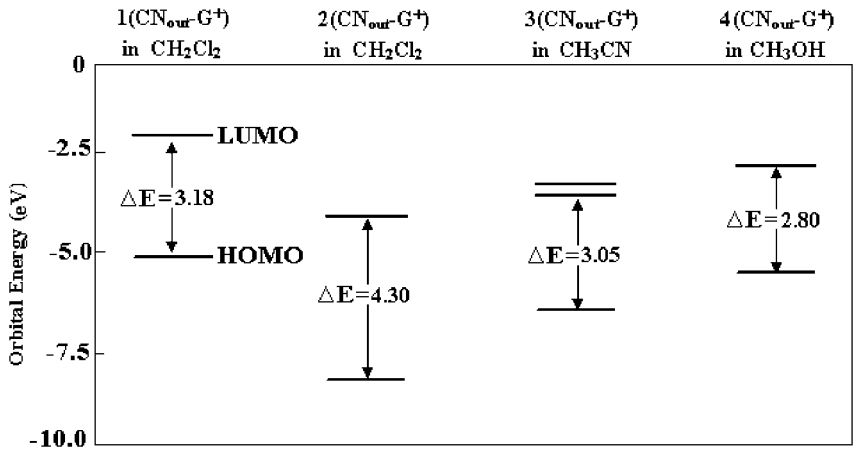

Fig. 5. Energy levels of frontier orbitals and the HOMO–LUMO gap, ΔE, in macrocycle **1**, **1**(CN_{out}-G^+) in CH_2Cl_2, and in zinc complexes **2**(CN_{out}-G^+) in CH_2Cl_2, **3**(CN_{out}-G^+) in CH_3CN, and **4**(CN_{out}-G^+) in CH_3OH, based on TDDFT-PCM calculations.

acterized by the local geometry of the bridged carbon moiety of the zinc complexes. Because of the delocalization of the HOMO, the orbital energy of **2** was much lower. Thus, the HOMO–LUMO gap of complex **2** is larger than that of the complexes **1**, **3**, and **4**. The transition energies are closely related to the HOMO–LUMO gap. Therefore, the discussion mentioned above gives a basic explanation about the reason why complex **2** alone showed no peaks at wavelengths longer than 330 nm.

Concluding Remarks

Geometry searches of stable conformers of the tetra-aza macrocycle and its zinc complexes were performed systematically. The relative energies and geometric features were compared and analyzed among the conformers. The optimized geometries were found to be consistent with the structural formula expected from the experimental results. Solvent effects were included in the calculations by using TDDFT-PCM. The calculated transition energies agreed with the experimental spectra in all the species except for a few cases. The difference in the transition energies was analyzed on the basis of the MO characters and orbital energies.

The authors thank the Research Center for Computational Science in Okazaki, Japan, for the use of the computer facilities.

References

1 D. T. McQuade, A. E. Pullen, T. M. Swager, *Chem. Rev.* **2000**, *100*, 2537, and the references therein.

2 S. Ogawa, R. Narushima, Y. Arai, *J. Am. Chem. Soc.* **1984**, *106*, 5760.

3 S. Ogawa, T. Uchida, T. Hirano, M. Saburi, Y. Uchida, *J. Chem. Soc., Perkin Trans. 1* **1990**, 1649.

4 S. Ogawa, S. Tsuchiya, *Chem. Lett.* **1996**, 709.

5 R. Ibrahim, S. Tsuchiya, S. Ogawa, *J. Am. Chem. Soc.* **2000**, *122*, 12174.

6 K. Takano, A. Furuhama, S. Ogawa, S. Tsuchiya, *J. Chem. Soc., Perkin Trans. 2* **1999**, 1063.

7 A. Furuhama, K. Takano, S. Ogawa, S. Tsuchiya, *Bull. Chem. Soc. Jpn.* **2001**, *74*, 1241.

8 A. Furuhama, K. Takano, S. Ogawa, S. Tsuchiya, *THEOCHEM* **2003**, *620*, 49.

9 J. J. P. Stewart, *J. Comput. Chem.* **1989**, *10*, 209.

10 a) J. S. Binkley, J. A. Pople, W. J. Hehre, *J. Am. Chem. Soc.* **1980**, *102*, 939. b) K. D. Dobbs, W. J. Hehre, *J. Comput. Chem.* **1987**, *8*, 861.

11 a) R. Ditchfield, W. J. Hehre, J. A. Pople, *J. Chem. Phys.* **1971**, *54*, 724. b) W. J. Hehre, R. Ditchfield, J. A. Pople, *J. Chem. Phys.* **1972**, *56*, 2257. c) P. C. Hariharan, J. A. Pople, *Theor. Chim. Acta* **1973**, *28*, 213. d) V. A. Rassolov, J. A. Pople, M. A. Ratner, T. L. Windus, *J. Chem. Phys.* **1998**, *109*, 1223.

12 a) A. D. Becke, *J. Chem. Phys.* **1993**, *98*, 5648. b) P. J. Stephens, C. F. Devlin, C. F. Chabalowski, M. J. Frisch, *J. Phys. Chem.* **1994**, *98*, 11623. c) C. Lee, W. Yang, R. G. Parr, *Phys. Rev. B* **1988**, *37*, 785.

13 S. H. Vosko, L. Wilk, M. Nusair, *Can. J. Phys.* **1980**, *58*, 1200.

14 C. Jamorski, M. E. Casida, D. R. Salahub, *J. Chem. Phys.* **1996**, *104*, 5134.

15 *BioMedCAChe Active Site V6*, Copyright(C) FUJITSU Limited Tokyo Japan, **2003**.

16 M. J. Frisch, G. W. Trucks, H. B. Schlegel, G. E. Scuseria, M. A. Robb, J. R. Cheeseman, J. A. Montgomery, Jr., T. Vreven, K. N. Kudin, J. C. Burant, J. M. Millam, S. S. Iyengar, J. Tomasi, V. Barone, B. Mennucci, M. Cossi, G. Scalmani, N. Rega, G. A. Petersson, H. Nakatsuji, M. Hada, M. Ehara, K. Toyota, R. Fukuda, J. Hasegawa, M. Ishida, T. Nakajima, Y. Honda, O. Kitao, H. Nakai, M. Klene, X. Li, J. E. Knox, H. P. Hratchian, J. B. Cross, C. Adamo, J. Jaramillo, R. Gomperts, R. E. Stratmann, O. Yazyev, A. J. Austin, R. Cammi, C. Pomelli, J. W. Ochterski, P. Y. Ayala, K. Morokuma, G. A. Voth, P. Salvador, J. J. Dannenberg, V. G. Zakrzewski, S. Dapprich, A. D. Daniels, M. C. Strain, O. Farkas, D. K. Malick, A. D. Rabuck, K. Raghavachari, J. B. Foresman, J. V. Ortiz, Q. Cui, A. G. Baboul, S. Clifford, J. Cioslowski, B. B. Stefanov, G. Liu, A. Liashenko, P. Piskorz, I. Komaromi, R. L. Martin, D. J. Fox, T. Keith, M. A. Al-Laham, C. Y. Peng, A. Nanayakkara, M. Challacombe, P. M. W. Gill, B. Johnson, W. Chen, M. W. Wong, C. Gonzalez, J. A. Pople, *Gaussian 03, Revision B.03*, Gaussian, Inc., Pittsburgh PA, **2003**.

17 H. Takahara, H. Nonomura, T. Kameyama, E. Nakano, S. Doi, Y. Tsuwa, *NEC Res. & Develop.* **1998**, *39*, 456.

18 D. Guillaumont, S. Nakamura, *Dyes Pigm.*, **2000**, *46*, 85.